Journal of Power Sources 196 (2011) 90–97

Contents lists available at ScienceDirect

Journal of Power Sources

journal homepage: www.elsevier.com/locate/jpowsour

Lithium and lanthanum promoted Ni-Al_2O_3 as an active and highly coking resistant catalyst layer for solid-oxide fuel cells operating on methane

Wei Wang, Ran Ran, Zongping Shao*

State Key Laboratory of Materials-Oriented Chemical Engineering, College of Chemistry & Chemical Engineering, Nanjing University of Technology, No.5 Xin Mofan Road, Nanjing 210009, PR China

ARTICLE INFO

Article history:
Received 25 May 2010
Received in revised form 9 July 2010
Accepted 12 July 2010
Available online 17 July 2010

Keywords:
Solid-oxide fuel cells
Anode
Catalyst layer
Methane
Carbon deposition

ABSTRACT

Ni-Al_2O_3 catalyst is modified with Li_2O_3, La_2O_3 and CaO promoters to improve its resistance to coking. These catalysts are used as the materials of the anode catalyst layer in solid-oxide fuel cells operating on methane. Their catalytic activity for the partial oxidation, steam reforming and CO_2 reforming of methane at 600–850 °C is investigated. Their catalytic stability and carbon deposition properties are also studied. The LiLaNi-Al_2O_3 catalyst shows a catalytic activity that is comparable to those of LaNi-Al_2O_3 and LiNi-Al_2O_3 catalysts for all three reactions. However, it displays a higher catalytic activity than those of CaLaNi-Al_2O_3 and CaNi-Al_2O_3 catalysts. Among the various catalysts, the LiLaNi-Al_2O_3 catalyst presents the highest catalytic stability. O_2-TPO profiles indicate that the modification of the Ni-Al_2O_3 catalyst with Li and La greatly reduces carbon deposition under pure methane atmosphere. The LiLaNi-Al_2O_3 catalyst is applied as the anode functional layer of a Ni + ScSZ anode-supported fuel cell. The cell is operated on methane-O_2, methane-H_2O or methane-CO_2 gas mixtures and yields peak power densities of 538, 532 and 529 mW cm^{-2} at 850 °C, respectively, comparable to that of hydrogen fuel. In sum, the LiLaNi-Al_2O_3 is highly promising as a highly coking resistant catalyst layer for solid-oxide fuel cells.

1. Introduction

Fuel cells are electrochemical energy conversion devices that directly convert chemical energy into electric power with high efficiency and low emissions. Solid-oxide fuel cells (SOFCs) have all-solid components and operate at elevated temperatures with fuel flexibility. Besides hydrogen, more accessible chemicals such as hydrocarbons, ammonia and coal are all potential fuels of SOFCs [1–5]. Methane, the simplest hydrocarbon, is the main component of natural gas and coal-bed gas and the renewable resource of biogas. It is not only less expensive and more easily and safely stored than hydrogen but also more readily accessible. The utilization of methane in SOFC technology has a great practical importance in the reduction of energy consumption and green house emissions.

SOFCs can operate on methane fuel according to three main operation modes. Pure methane can be directly fed into the fuel cell anode where it is electrocatalytically oxidized into CO_2 and H_2O ($CH_4 + 4O^{2-} \rightarrow CO_2 + 2H_2O + 8e^-$) without intermediate reforming processes. Such types of fuel cells are called direct-methane SOFCs [6–9]. The main advantage of this operation mode is its simplicity. However, it also presents two main drawbacks, i.e., an easy coke formation over the nickel cermet anode ($CH_4 \rightarrow C + 2H_2$) and a poor cell performance, which greatly inhibits the practical application of direct-methane SOFCs. Recently, considerable research efforts have been expended on the development of non-nickel anode materials with improved coking resistivity and high activity for direct electrochemical oxidation of methane [10–13]. However, the progress is still slow up to now, especially in increasing the power output at reduced temperatures. Another way to operate SOFCs on methane is to first convert methane into hydrogen by external reforming ($CH_4 + 2H_2O \rightarrow CO_2 + 4H_2$) [14–17]. In this operation mode, the actual fuel for the electrochemical oxidation over the fuel cell anode is hydrogen instead of methane. The advantages of this operation mode are that the conventional cermet anode can still be applied and that the cell performance is comparable to that operating on hydrogen. However, the external reforming greatly increases the complexity of the fuel cell system. Furthermore, the steam reforming of methane is highly energy intensive, which reduces the overall fuel efficiency. The internal reforming (or partial oxidation) of methane over the SOFC anode has recently attracted considerable attention [18–25]. In this operation mode, a gas mixture consisting of methane and steam (or CO_2 or O_2) is fed into the fuel cell anode, which performs as the catalyst for the steam reforming (partial oxidation) of methane to syngas. The advantages of internal reforming (partial oxidation) include a simpler operation mode and an easier thermal management than external reforming, and a higher cell performance and decreased sensitivity to coke formation than the direct-methane SOFCs.

* Corresponding author. Tel.: +86 25 83172256; fax: +86 25 83172256.
E-mail address: shaozp@njut.edu.cn (Z. Shao).

0378-7753/$ – see front matter © 2010 Elsevier B.V. All rights reserved.
doi:10.1016/j.jpowsour.2010.07.033

However, the state-of-the-art sintered nickel cermet anode has a poor catalytic activity towards methane and steam/CO_2 reforming and partial oxidation, especially at reduced temperatures; in addition, coke is easily formed over the sintered nickel cermet. The development of alternative anodes is therefore critical for the SOFC technology that is based on the internal reforming (partial oxidation) of methane. The modification of conventional SOFC cermet anodes is more practical than the development of totally new anode materials due to its simplicity. Recently, the deposition of a layer of a catalyst possessing a high activity for the reforming (partial oxidation) of methane and a good resistance towards coke formation on a conventional cermet anode was proposed to increase the operational stability and performance of hydrocarbon-fueled SOFCs [26–28]. In this operation mode, hydrocarbons first pass through the functional layer where they are converted to syngas ($CO + H_2$) over the catalyst layer. Thus, as hydrocarbons are converted before they can reach the anode, and the conventional anode is well protected from carbon deposition. Barnett and colleagues have first demonstrated that Ru-CeO_2 can be used as the catalyst layer [26]. The cell power output and anode coke resistance of fuel cells with a Ru-CeO_2 functional layer were obviously better than those of cells without a catalyst layer and operating on methane, propane or octane fuels [26,29,30]. However, the high cost of Ru is a handle for SOFC application.

In our previous work, we have demonstrated that an inexpensive Ni-Al_2O_3 catalyst has a catalytic activity for the partial oxidation, steam reforming, and CO_2 reforming of methane between 600 and 850 °C that is comparable to that of Ru-CeO_2 [31,32]. Furthermore, the Ni-Al_2O_3 catalyst layer showed a much better mechanical performance than Ru-CeO_2. However, Ni-Al_2O_3 is still prone to coke formation even though only a small amount of carbon was deposited over the Ni-Al_2O_3 catalyst layer in a real fuel cell after operation on methane for a period of 2.5 h which was due to the low nickel loading in the Ni-Al_2O_3 catalyst. Thus, the coke resistance of the functional layer must still be improved for long-term operations.

It is well known that the catalytic activity and coking resistivity of nickel catalysts is strongly influenced by the support and the promoters. Some lanthanum ions or alkaline metal ions were found to be good promoters for nickel catalysts to obtain improved catalytic activity and carbon resistance [33–39]. For example, it was reported that Li and La-modified Ni catalysts that were supported on γ-Al_2O_3 had a high catalytic activity for the partial oxidation of methane [40–42].

To further increase the catalytic activity for the internal reforming of methane (partial oxidation) and coke resistance of the functional layer, La_2O_3, Li_2O and CaO were selected in this study as promoters for the Ni-Al_2O_3 catalysts. A comparative study of various catalysts for the steam reforming, CO_2 reforming and partial oxidation of methane between 600 and 850 °C is presented herein. Finally, the performance of the Li and La-modified Ni-Al_2O_3 catalyst as the functional layer on the anode in a fuel cell operating on methane was studied.

2. Experimental

2.1. Synthesis and fabrication

All the catalyst powders investigated in this study as the materials for the catalyst layer were synthesized by a glycine nitrite process (GNP) [43]. Taking the synthesis of the Li and La co-promoted Ni-Al_2O_3 catalyst as an example, stoichiometric amounts of nickel nitrate, lanthanum nitrate, lithium nitrate and alumina nitrate were dissolved in de-ionized water to form a solution; glycine was then added at a molar ratio of glycine to total metallic cations of 2. The solution was heated on a hot plate under stirring to evaporate water until a gel precursor was obtained. This gel precursor was then transferred to a pre-heated electric oven at 240 °C to initialize auto-combustion. The as-resulted primary powder was further calcined at 850 °C for 5 h in static air. After cooling to room temperature, the powder was pressed into disks and crashed to small pellets with desired particle size for catalytic tests.

The fuel cell materials, including the cathode $La_{0.8}Sr_{0.2}MnO_3$ (LSM) and the electrolyte $(Sc_2O_3)_{0.1}(ZrO_2)_{0.9}$ (ScSZ), were prepared by an EDTA-citrate complexing process [44]. The fuel cell used in this study was a 60 wt.% NiO + 40 wt.% ScSZ cermet anode-supported thin-film ScSZ electrolyte fuel cell (~20 μm), fabricated by a dual dry-pressing/sintering process. The NiO + ScSZ anode powder was first pressed into a substrate disk using a stainless steel die under a hydraulic pressure of 120 MPa. Ultrafine ScSZ powder with a low packing density was then homogenously distributed over the anode surface and a second press under a pressure of 240 MPa was applied to form a green dual layer cell that was sintered at 1500 °C for 5 h to densify the electrolyte layer. The sintered cells had a diameter of ~13 mm and a thickness of ~0.3 mm.

To prepare the catalyst layer, a slurry of the catalyst powder was prepared, painted onto the outer surface of the anode layer, and sintered at 850 °C in air for 1 h.

2.2. Catalytic evaluation

The catalytic activity of the various nickel-based catalysts was studied in a flow-through type of a fixed-bed, quartz-tube reactor with an inner diameter of ~8 mm. The test was performed between 600 and 850 °C. About 0.2 g of catalyst particles having a size of 60–80 mesh were put in the middle of the reactor. Gas mixtures were fed into the reactors at a flow rate of $CH_4/O_2/He = 10/5/80$, $CH_4/H_2O/He = 10/10/80$ and $CH_4/CO_2/He = 10/10/80$ ml min^{-1} [STP] for the partial oxidation, steam reforming and CO_2 reforming of methane, respectively. The flow rate was controlled using AFC 80MD digital mass flow controllers (Qualiflow). The gas mixtures were introduced from the top of the reactor; the effluent gases at the bottom of the reactor were introduced to a Varian 3800 gas chromatograph, which was equipped with Hayesep Q, Poraplot Q and 5 Å sieve molecular capillary columns and a thermal conductivity detector (TCD) for the separation and detection of H_2, O_2, CO, CO_2 and CH_4 species. Conversion of methane (X (%)) during partial oxidation, steam reforming and CO_2 reforming was calculated according to the following equations:

$$X(\%) = \frac{[CO] + [CO_2]}{[CO] + [CO_2] + [CH_4]} \times 100\% \quad (1)$$

$$X(\%) = \frac{0.5[CO]}{0.5[CO] + [CH_4]} \times 100\% \quad (2)$$

While the selectivity of CO (S (%)) was calculated according to:

$$S(\%) = \frac{[CO]}{[CO] + [CO_2]} \times 100\% \quad (3)$$

2.3. Other characterizations

The phase structures of the various catalysts were examined using an X-ray diffractometer (XRD, ARL X' TRA) equipped with a Cu Kα radiation (λ = 0.1541 nm). The BET specific surface area of the catalysts was characterized by N_2 adsorption at liquid nitrogen temperature using a surface area analyzer (BELSORP II, Japan). Prior to nitrogen adsorption, the sample was degassed at 300 °C for 2.0 h to remove any physically adsorbed species. The surface area was determined from the linear portion of the BET equation. The cross-sectional morphologies of the fuel cells were examined using

an environmental scanning electron microscope (ESEM, QUANTA-200).

Hydrogen temperature-programmed reduction (H_2-TPR) was performed to identify the interaction between NiO and the support (promoter). Approximately 0.03 g of 60–80 mesh catalyst powder was placed in a U-type quartz reactor with an inner diameter of ~3 mm. The sample was pretreated under a pure argon atmosphere at a flow rate of 30 ml min^{-1} for 30 min. After cooling to room temperature, the gas was switched to a gas mixture of 10 vol.% H_2 in argon, and then the reactor was heated to 930 °C at a rate of 10 °C min^{-1}. The consumption of hydrogen was monitored by an on-line TCD detector using a BELCAT-A apparatus (Japan).

To test the coke resistivity of the various catalysts, about 0.05 g of catalyst after the treatment in various methane-contained atmospheres for a certain period were placed into a U-type quartz reactor with an inner diameter of ~3 mm. Pure oxygen (for oxygen temperature-programmed oxidization, O_2-TPO) at a flow rate of 20 ml min^{-1} [STP] was then introduced from the top of the reactor. After flowing ~30 min at room temperature, the reactor was heated to 800 °C at a rate of 10 °C min^{-1}. The deposited carbon on the catalyst surface was gradually oxidized to CO_2. The effluent gas from the reactor was connected to a Hiden QIC-20 Mass Spectroscope (MS) for in situ monitoring of the CO_2 concentration variation.

2.4. Electrochemical characterization

The cell performance was characterized by *I–V* and *I–P* polarization. The fuel cell was first sealed onto a quartz tube and was then slowly heated to 850 °C using an electric furnace. During the heating process, both the anode and cathode were exposed to ambient air. After stabilization at 850 °C for several hours, the anode atmosphere was changed to fuel gas, i.e., pure methane or a gas mixture containing either CH_4–O_2, CH_4–CO_2 or CH_4–H_2O, at a flow rate of 40 ml min^{-1} [STP]. The *I–V* and *I–P* polarization tests were performed in 4-probe mode and the curves were recorded using a Keithley 2420 source meter. After the test at 850 °C was completed, the temperature was dropped to another temperature for *I–V* and *I–P* tests. The measurement was conducted at 25 °C per step until 750 °C.

3. Results and discussion

3.1. Basic properties

An ideal material for the catalyst layer of SOFCs operating on methane should have a high activity for the partial oxidation, steam reforming and CO_2 reforming of methane. We have previously demonstrated that a Ni-Al_2O_3 (7 wt.% Ni) catalyst prepared by a glycine-nitrate combustion process had a good activity for the afore-mentioned three reactions at intermediate temperatures. To further improve the catalytic performance, La_2O_3, Li_2O and CaO were applied as promoters to modify the Ni-Al_2O_3 catalyst. Five new catalysts, i.e., LiLaNi-Al_2O_3, LaNi-Al_2O_3, LiNi-Al_2O_3, CaLaNi-Al_2O_3 and CaNi-Al_2O_3 were thus prepared by the same glycine-nitrate combustion method. For the GNP, the combustion is in a self-propagated manner, therefore, in some cases, the reaction may be not well controllable. However, by precisely controlling the reaction parameters, the reaction could be made with good repeatability. For example, the oxidation–reduction reaction is sensitive to the ratio of glycine to cations [45]. The flame temperature is strongly affected by the ratio of glycine to metal [46,47]. During the experiment, the ratio of glycine to metal was strictly kept at 2.0 for all the catalysts. To ensure the high homogeneity of the catalyst, the as-obtained catalyst from the GNP was further conducted the calcination at 850 °C for 5 h. For comparison, Ni-Al_2O_3 was also synthesized. After the direct combustion synthesis, all the catalysts were further calcined at 850 °C for 5 h in air. Details about the catalyst compositions are listed in Table 1. In all catalysts, the nickel content was fixed at 7 wt.% and the molar ratio of the total amount of promoters to the amount of nickel was fixed at 0.82:1. The XRD results are shown in Fig. 1. As can be seen, the γ-Al_2O_3 crystalline phase was detected for all samples. No other phase, including NiO, was observed. These results suggest that La, Li and Ca were all well dispersed within the catalysts.

Table 1
The details about the catalyst compositions.

Catalysts	The contents of the promoters and nickel
LiLaNi-Al_2O_3	1 wt.% Li_2O, 5 wt.% La_2O_3 and 7 wt.% nickel
LaNi-Al_2O_3	15.9 wt.% La_2O_3 and 7 wt.% nickel
LiNi-Al_2O_3	1.46 wt.% Li_2O and 7 wt.% nickel
CaLaNi-Al_2O_3	3.75 wt.% CaO, 5 wt.% La_2O_3 and 7 wt.% nickel
CaNi-Al_2O_3	5.47 wt.% CaO and 7 wt.% nickel

The specific surface areas of the catalysts were measured by the nitrogen adsorption method at liquid nitrogen temperature. The values for the specific surface areas were 66.7, 16.2, 40.8, 16.4, 14.3 and 48.0 m^2 g^{-1} for LiLaNi-Al_2O_3, LaNi-Al_2O_3, LiNi-Al_2O_3, CaLaNi-Al_2O_3, CaNi-Al_2O_3 and Ni-Al_2O_3, respectively. It is obvious that the promoters and their concentrations influenced the specific surface area of each catalyst. El-shobaky et al. have demonstrated that the BET specific surface area slightly decreases with an increasing amount of Li_2O for Li_2O-promoted Ni-Al_2O_3 catalysts [48]. Our results are well in agreement with their findings even though different catalysts and synthetic techniques were applied in both cases. It is interesting that LiLaNi-Al_2O_3 had the highest specific surface area, while LaNi-Al_2O_3 had the lowest. Chen et al. studied in detail the effect of La_2O_3 on the specific surface area of the Al_2O_3 support [49]. They found that the surface area is closely related to the so-called atomic ratio of lanthanum to aluminum (La/Al). Indeed, for La/Al ≤ 0.02, the specific surface area of the La_2O_3-promoted Al_2O_3 samples was higher than that of the pure Al_2O_3 sample after calcination at the same temperature. The maximum specific surface area was achieved at a La/Al atomic ratio of 0.02. For La/Al ≥ 0.05, the specific surface areas of the La_2O_3-promoted aluminum samples decreased rapidly with the increase of the La/Al atomic ratio and the specific surface area of the samples with high La/Al atomic ratio started to be lower than that of the pure Al_2O_3 sample. In our work, the La/Al atomic ratios of LiLaNi-Al_2O_3 and LaNi-Al_2O_3 were 0.02 and 0.064, respectively. The above-mentioned theory explains

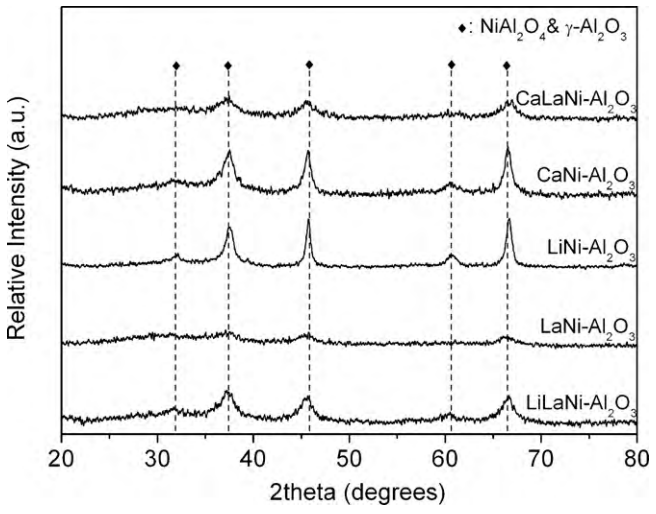

Fig. 1. XRD patterns of the combustion-synthesized LiLaNi-Al_2O_3, LaNi-Al_2O_3, LiNi-Al_2O_3, LaCaNi-Al_2O_3, and CaNi-Al_2O_3 catalysts after firing at 850 °C.

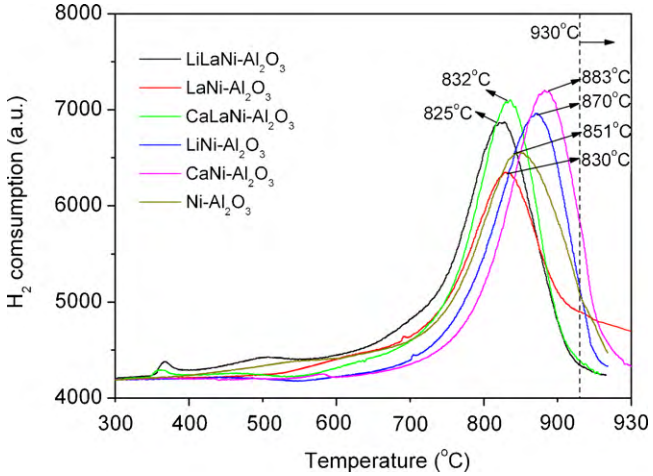

Fig. 2. Profiles of H_2 temperature-programmed reduction of LiLaNi-Al_2O_3, LaNi-Al_2O_3, LiNi-Al_2O_3, LaCaNi-Al_2O_3, CaNi-Al_2O_3 and Ni-Al_2O_3 catalysts.

why the specific surface area of LiLaNi-Al_2O_3 was higher than that of LaNi-Al_2O_3. The CaO-promoted Ni-Al_2O_3 catalysts had a much lower BET specific surface area than that of the Ni-Al_2O_3 catalyst. The higher the CaO content was, the lower the surface area of the CaO-promoted Ni-Al_2O_3 catalysts was. A similar effect of CaO on the specific surface area of Ni-Al_2O_3 based catalysts was previously reported in the literature [50]. It was proposed that the reduced specific surface area observed in the case of the introduction Ca was due to the interaction between CaO and the Al_2O_3 support, which may result in the formation of $CaAl_4O_7$ [51].

The catalytic activity and coke resistivity of nickel-based catalysts for the partial oxidation of methane is also closely related to the interaction between nickel and the support [52]. The chemical interaction between nickel and the support and/or the promoters was characterized by H_2-TPR. Fig. 2 shows the H_2-TPR profiles of the various catalysts. The reduction peak temperature of free NiO during the H_2-TPR process was reported to be around 330 °C [53]. With the increase of the chemical interaction between NiO and the support or promoters, a shift of the reduction peak to higher temperatures was expected. The reduction peak temperatures of the six catalysts were all higher than 800 °C, thereby suggesting that there was a strong interaction between nickel and the support (γ-Al_2O_3) or the promoters in the various catalysts synthesized by the glycine-nitrate combustion process. Such interaction could effectively suppress the grain growth of the NiO phase, which is beneficial for increasing the catalytic activity of the catalysts. A slight difference in peak temperatures was observed for the various catalysts with different promoters. The reduction peak temperatures of the three La_2O_3-promoted catalysts, i.e., LiLaNi-Al_2O_3, LaNi-Al_2O_3 and CaLaNi-Al_2O_3, were around 830 °C, which is slightly lower than that of Ni-Al_2O_3 (851 °C). The reduction peak temperatures of the LiNi-Al_2O_3 and CaNi-Al_2O_3 catalysts were the highest at 870 and 883 °C, respectively. The relatively low reduction peak temperature of the La_2O_3-promoted catalysts can be explained by the formation of the $LaNiO_{2.5}$ perovskite-related oxide, which has a lower stability than the Ni_2AlO_4 spinel [54]. The higher reduction temperatures of the CaNi-Al_2O_3 and LiNi-Al_2O_3 catalysts as compared with the Ni-Al_2O_3 catalyst suggests that the introduction of Li or Ca promoters increases the interaction of Ni with the support and/or promoter. The increased reduction temperature of the Ni-Al_2O_3 catalyst by the addition of Li_2O or CaO was previously reported by other researchers [55,56]. Hou et al. have demonstrated that an additional reduction peak around 400 °C appears for a CaNi-Al_2O_3 catalyst at a high CaO concentration; this can be attributed to the reduction of free NiO particles within the catalyst [56]. In our

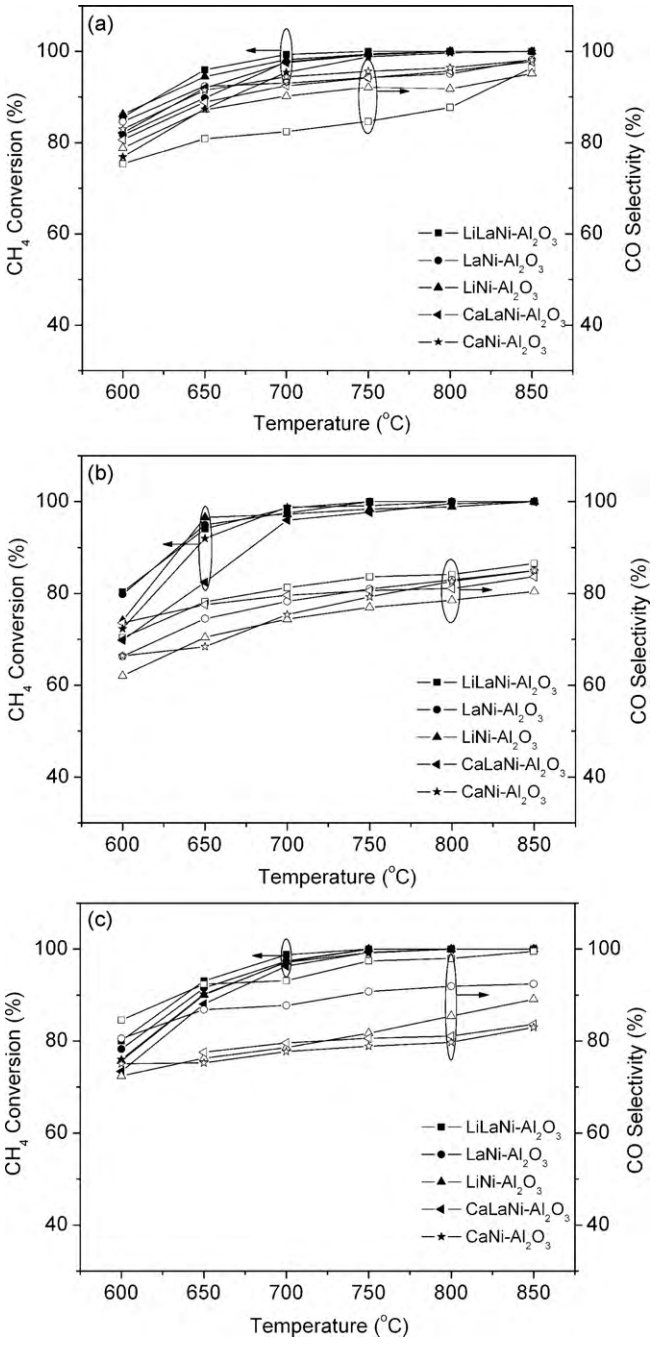

Fig. 3. Catalytic activity of LiLaNi-Al_2O_3, LaNi-Al_2O_3, LiNi-Al_2O_3, LaCaNi-Al_2O_3 and CaNi-Al_2O_3 catalysts for (a) partial oxidation (CH_4:O_2 = 2:1), (b) steam reforming (CH_4:H_2O = 1:1) and (c) CO_2 reforming (CH_4:CO_2 = 1:1).

study, no such peak appeared, thereby implying that the combustion synthesis resulted in a better and more homogeneous chemical interaction between NiO and the Al_2O_3 support than that of the catalyst prepared by the conventional wetness co-impregnation method.

3.2. Catalytic performance

Fig. 3 shows the methane conversion and CO selectivity over LiLaNi-Al_2O_3, LaNi-Al_2O_3, LiNi-Al_2O_3, CaLaNi-Al_2O_3 and CaNi-Al_2O_3 catalysts for the partial oxidation, steam reforming and CO_2 reforming of methane at the methane to oxygen/H_2O/CO_2 ratio of 2:1, 1:1 and 1:1, respectively. All five catalysts showed a favor-

Table 2
Methane conversion during the partial oxidation, steam reforming, and CO_2 reforming of methane at 600 °C over LiLaNi-Al_2O_3, LaNi-Al_2O_3, LiNi-Al_2O_3, CaLaNi-Al_2O_3 and CaNi-Al_2O_3 catalysts.

Catalysts	CH_4 conversion		
	Partial oxidation	Steam reforming	CO_2 reforming
LiLaNi-Al_2O_3	85.6%	80.3%	80.0%
LaNi-Al_2O_3	81.7%	79.7%	78.2%
LiNi-Al_2O_3	86.2%	74.1%	75.6%
CaLaNi-Al_2O_3	82.1%	69.8%	73.4%
CaNi-Al_2O_3	76.8%	72.3%	75.9%

able catalytic activity for the above-mentioned three reactions at high temperatures (750–850 °C). The decrease of the operation temperature led to different activities. Table 2 lists the detailed methane conversion over the five catalysts at 600 °C. It shows that the catalytic activity of the CaO-promoted Ni-Al_2O_3 catalysts is a little lower than that of the Li_2O-promoted and La_2O_3-promoted Ni-Al_2O_3 catalysts. For example, the CH_4 conversion over the LiLaNi-Al_2O_3 catalyst reached 85.6%, 80.3% and 80.0% for reactions 1, 2 and 3, respectively, while they were 82.1%, 69.8% and 73.4% over the CaLaNi-Al_2O_3 catalyst.

The catalyst layer of SOFCs must also display high operation stability. Methane conversion over the various catalysts was first carried out under methane-rich conditions, i.e., at CH_4:O_2 = 11.5:1, at 850 °C for a period of 100 h. The CO selectivity of 100% was achieved for all catalysts due to the high methane to oxygen ratio. Fig. 4 indicates the dependence of the methane conversion on the operation time for the various catalysts. After 100 h of operation, the decrease in methane conversion was of 4.5%, 4.6%, 5.8%, 6.7% and 7.6% for the LaNi-Al_2O_3, LiNi-Al_2O_3, CaLaNi-Al_2O_3, CaNi-Al_2O_3 and Ni-Al_2O_3 catalysts, respectively. The Ni-Al_2O_3 catalyst presented the worst catalytic stability. In general, the catalytic stability of the Ni-Al_2O_3 catalysts was improved by introducing the various promoters. However, the improvement was different for different compositions. During the first 20 h of operation, the performance of all six catalysts was relatively stable. However, during the next 80 h of operation, the decrease of the methane conversion varied for the different catalysts. The methane conversion over the CaNi-Al_2O_3 and Ni-Al_2O_3 catalysts decreased rapidly, while it was found to be stable over the LiLaNi-Al_2O_3 catalyst during the whole operation period. The catalytic deactivation of γ-$A1_2O_3$-supported catalysts during high-temperature operations is typically due to the thermal

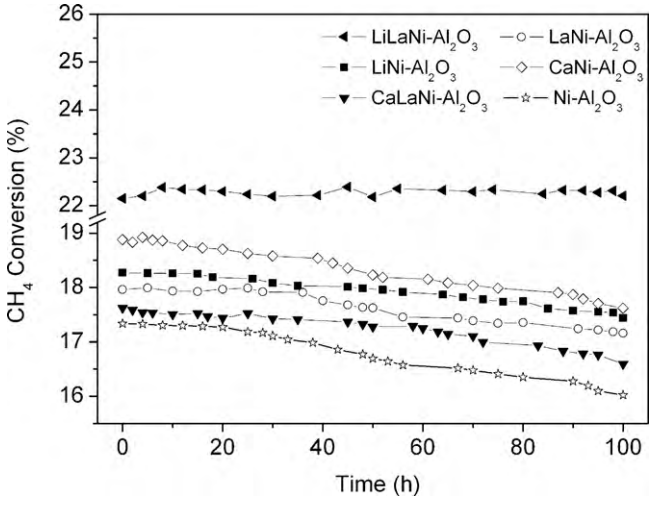

Fig. 4. Time dependence of methane conversion under CH_4:O_2 = 11.5:1 conditions for LiLaNi-Al_2O_3, LaNi-Al_2O_3, LiNi-Al_2O_3, LaCaNi-Al_2O_3, CaNi-Al_2O_3 and Ni-Al_2O_3 catalysts.

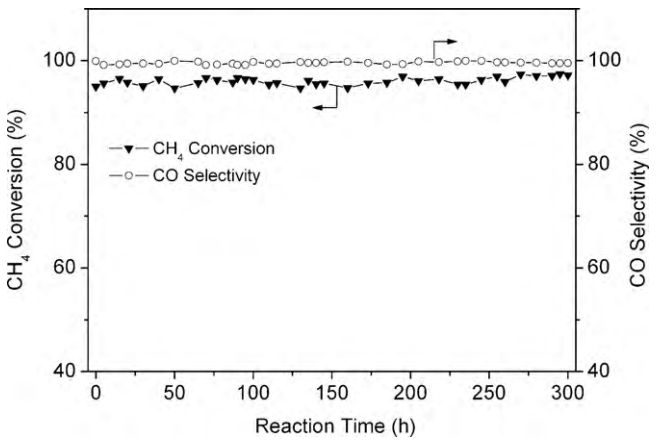

Fig. 5. Time dependence of methane conversion and CO selectivity under CH_4:O_2 = 2.2:1 conditions for the LiLaNi-Al_2O_3 catalyst.

deterioration of the γ-$A1_2O_3$ support, i.e., the sintering and phase transformation into α-$A1_2O_3$ that has a low surface area structure [57]. Rare earth metal oxides could prevent the alumina support from thermal deterioration [58]. The influence of alkali metals on the Lewis acid sites of γ-$A1_2O_3$ has been studied by NMR and IR of adsorbed CO by Castro and co-workers [59]. It was found that the alkali metals could not only introduce steric effects but also possible electronic modifications. The higher operation stability of the LiLaNi-Al_2O_3 catalyst, as compared with the LiNi-Al_2O_3 and LaNi-Al_2O_3 catalysts, implies that La and Li oxides may have a synergistic effect on the Ni-Al_2O_3 catalyst, which results in an excellent catalytic activity and operation stability of the LiLaNi-Al_2O_3 catalyst.

To further evaluate the operation stability of the LiLaNi-Al_2O_3 catalyst under more real fuel cell operation conditions, the catalyst was used for the partial oxidation of methane under slightly methane-rich conditions, i.e., CH_4:O_2 = 2.2:1, at 850 °C for a period of 300 h. Fig. 5 shows the corresponding methane conversion and CO selectivity. The methane conversion was stable at ~95% and the CO selectivity was ~100% during the course of the 300 h of operation. The strong interaction between the NiO species and the Al_2O_3 support, as evidenced by the H_2-TPR results, largely contributed much to the excellent stability of the LiLaNi-Al_2O_3 catalyst by suppressing the sintering of the active nickel component.

3.3. Carbon deposition

The anode catalyst layer must also display a high resistance to coke formation. The formation of carbon over the catalyst layer may destroy the integrity of the functional layer and therefore fail to protect the anode layer. Methane would then be directly in contact with the nickel cermet anode. Coke formation over the anode would thus most likely occur as nickel catalyses the methane cracking reaction. The deposited carbon can block the active sites of the anode, leading to a rapid deterioration of the fuel cell performance.

To test the coke resistivity of the catalysts, the catalysts were subjected to a mixture of CH_4 and O_2 at a molar ratio of 11.5:1 for 100 h and O_2-TPO analyses were performed. Fig. 6 shows the O_2-TPO profiles of the catalysts. The order for the values of the CO_2 peak area of the different catalysts was: Ni-Al_2O_3 > LiNi-Al_2O_3 > LiLaNi-Al_2O_3 > CaLaNi-Al_2O_3 > LaNi-Al_2O_3 > CaNi-Al_2O_3. The amount of carbon deposited was calculated found to be 1.56E-5, 1.33E-5, 1.06E-5, 7.64E-6, 5.81E-6 and 5.12E-6 for Ni-Al_2O_3, LiNi-Al_2O_3, LiLaNi-Al_2O_3, CaLaNi-Al_2O_3, LaNi-Al_2O_3, and CaNi-Al_2O_3, respectively. These results indicate that the introduction of alkali metal and rare earth metal oxides to the Ni-Al_2O_3 catalyst increases the coking resistance of the catalyst. The CaO-promoted Ni-Al_2O_3 cat-

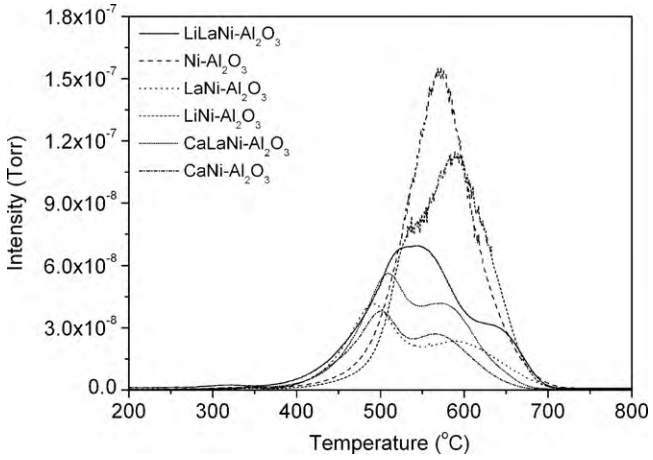

Fig. 6. O_2-TPO profiles of LiLaNi-Al_2O_3, LaNi-Al_2O_3, LiNi-Al_2O_3, LaCaNi-Al_2O_3, CaNi-Al_2O_3 and Ni-Al_2O_3 catalysts after operation under CH_4:O_2 = 11.5:1 conditions for 100 h.

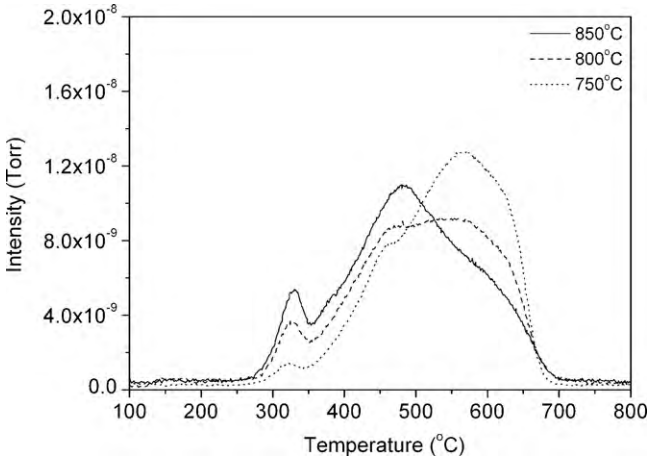

Fig. 7. O_2-TPO profiles of the LiLaNi-Al_2O_3 catalyst after treatment in pure methane for 5 min at 750–850 °C.

alysts had the best coking resistance among all the tested catalysts, while the Li_2O-promoted Ni-Al_2O_3 catalysts only slightly improved the coking resistance as compared with the Ni-Al_2O_3 catalyst. It is well known that an acidic catalyst surface favors carbon deposition, while a basic one suppresses carbon deposition [60]. The improvement in coke resistance by introduction of CaO, Li_2O or La_2O_3 promoters is most likely due to the increase of the basicity of the catalyst.

Under the methane-O_2/H_2O/CO_2 gas mixtures, the formation of coke and the elimination of coke happened simultaneously. The amount of carbon deposited on the catalyst depends on the difference between the coke formation rate and the coke elimination rate. To further exploit the coke resistance of the LiLaNi-Al_2O_3 catalyst, in the catalyst was first subjected to pure methane at various temperatures at a flow rate of 40 ml min^{-1} for 5 min. It was then protected with an inert gas at the flow rate of 40 ml min^{-1} at room temperature. Fig. 7 presents the O_2-TPO profiles of the LiLaNi-Al_2O_3 catalyst after treatment in pure methane at the temperature between 750 and 850 °C for 5 min. For comparison, the O_2-TPO profile of the Ni-Al_2O_3 catalyst after the same treatment

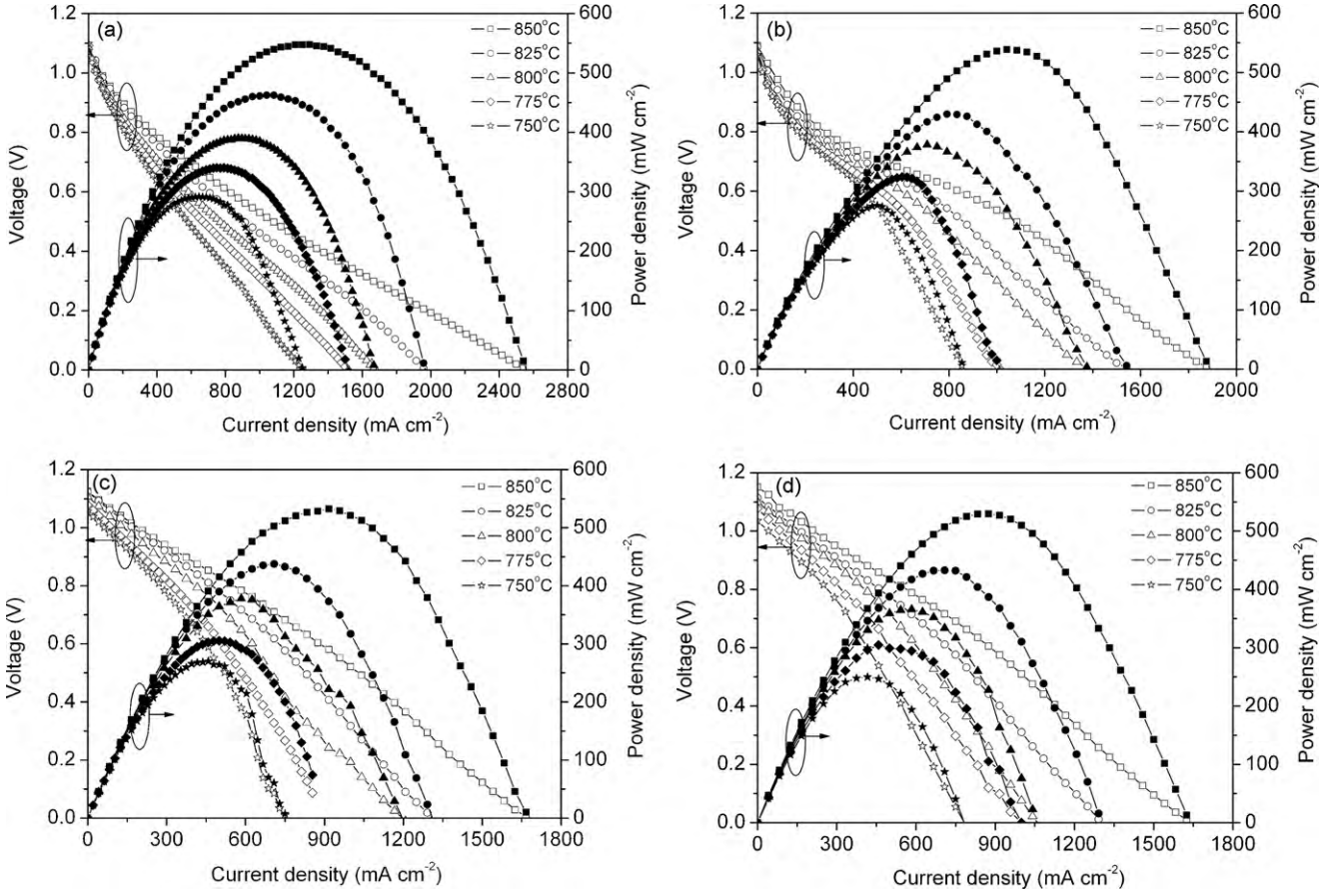

Fig. 8. *I–V* and *I–P* curves of the fuel cells with the LiLaNi-Al_2O_3 catalyst layer operating on a mixed gas composed of pure hydrogen (a), 80% CH_4 and 20% O_2 (b), 66.7% CH_4 and 33.3% H_2O (c) and 66.7% CH_4 and 33.3% CO_2 (d) at different temperatures.

at 850 °C is also presented [32]. The amount of carbon deposited over the LiLaNi-Al_2O_3 catalyst after the treatment in pure CH_4 gas for 5 min at 850 °C is only 18.5% as compared to that of Ni-Al_2O_3 [32]. This is in good agreement with literature results showing that the introduction of La and Li oxides can greatly improve the coking resistance of Ni-Al_2O_3 catalysts [42].

3.4. Cell performance

The LiLaNi-Al_2O_3 catalyst was investigated as the anode functional layer in a real fuel cell. An anode-supported thin-film electrolyte fuel cell with a ScSZ electrolyte, a LSM cathode and a LiLaNi-Al_2O_3 functional layer was prepared. Shown in Fig. 8 are the *I–V* and *I–P* curves of the fuel cell operating on a methane-oxygen gas mixture, methane-steam gas mixture, and methane-CO_2 gas mixture. The methane to oxygen/H_2O/CO_2 was 4:1, 2:1 and 2:1 at different temperatures. During the fuel cell operation, the methane and O_2/CO_2/H_2O were reacted over the catalyst layer to form synthesis gas, which diffused into the anode layer to provide the fuel for the electrocatalytic oxidation over the triple phase boundaries. By applying the methane-oxygen gas mixture as the fuel, the cell delivered peak power densities of 538, 430, 378, 324 and 276 mW cm^{-2} at 850, 825, 800, 775 and 750 °C, respectively, while they were 547, 462, 390, 340 and 291 mW cm^{-2} when pure hydrogen was applied as the fuel. This indicates that the cell power outputs are similar by operating on methane-oxygen fuel and hydrogen fuel. It was reported that the cell delivered similar power outputs by operating on CO and H_2 gas mixtures and pure hydrogen because the CO can react with H_2O to produce CO_2 and H_2 [61]. It implies that the methane was effectively converted to synthesis gas ($CO + H_2$) over the LiLaNi-Al_2O_3 catalyst layer before it reached the anode layer. Otherwise, a much lower cell power output should be expected since methane has an activity that is much lower than that of H_2. The cell delivered similar power outputs by operating on methane-steam or methane-CO_2 gas mixtures. These results indicate that the catalyst layer had a catalytic activity that was sufficient for the partial oxidation, steam reforming and CO_2 reforming of methane.

In our previous work, experiments on the stability of the cell performance with and without a Ni-Al_2O_3 catalyst layer were carried out. When no Ni-Al_2O_3 catalyst layer was adopted, the PPD was reduced to about 41% of the initial value after operation on methane stream for 90 min. The decrease in PPD was of just about 3% when Ni-Al_2O_3 catalyst layer was adopted; it was still of only 4% after the operation on pure methane fuel for about 150 min [31]. The operation stability test was also carried out on the cell with the LiLaNi-Al_2O_3 catalyst layer. As shown in Fig. 9, by applying pure methane as the fuel, the open circuit voltage of the cell was stable during the course of the test, i.e., during 150 min, with a value of ~1.17 V. The initial PPD of the fuel cell was 437 mW cm^{-2}. After 150 min of operation, the PPD decreased to 421 mW cm^{-2} with a reduction of only about 3.7%. Shown in Fig. 9b, the voltage is 0.694 V at the current density of 500 mA cm^{-2} at the beginning of the stability test, while the voltage decreased to 0.685 V with a reduction of only about 1.3% after 150 min of current polarization at 500 mA cm^{-2}. This good stability is a result of the good coking resistance of the LiLaNi-Al_2O_3 catalyst, as evidenced by the O_2-TPO results.

The SEM image of the fuel cell after the performance test between 750 and 850 °C under different fuel conditions for a period of 10 h is shown in Fig. 10. The catalyst layer still adhered to the anode surface pretty well without any delimitation. In addition, no carbon could be observed on the catalyst layer and the anode layer. The above results indicate that the LiLaNi-Al_2O_3 catalyst can be ideally used as the functional layer of SOFCs operating on methane fuel.

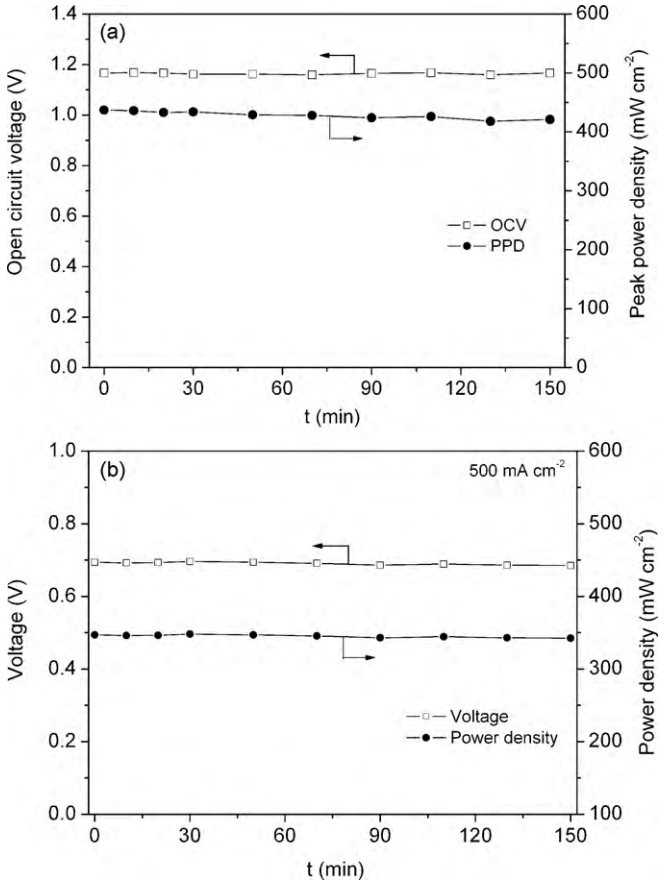

Fig. 9. Time dependence of the peak power density and open circuit voltage (a), and voltage and power density under a constant polarization current density of 500 mA cm^{-2} (b), of the fuel cell with the LiLaNi-Al_2O_3 catalyst layer operating on pure methane fuel.

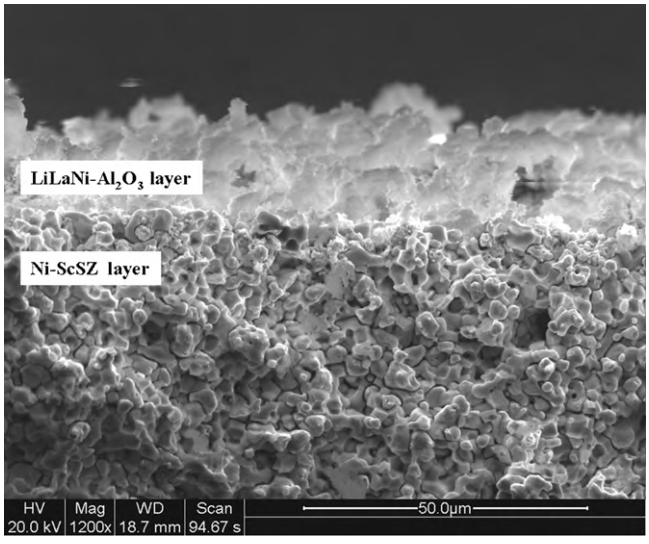

Fig. 10. Cross-sectional SEM images of the catalyst–anode interface after the operation on methane fuel.

4. Conclusions

The combustion-synthesized LiLaNi-Al_2O_3 catalyst had an excellent catalytic activity for the partial oxidation, steam reforming and CO_2 reforming of methane between 600 and 850 °C. Its catalytic activity was comparable to those of LaNi-Al_2O_3 and LiNi-

Al_2O_3 catalysts but was higher than those of CaLaNi-Al_2O_3 and CaNi-Al_2O_3 catalysts. The strong interaction between NiO and the support accounted for the high activity of all five catalysts. Catalyst stability tests showed that the LiLaNi-Al_2O_3 catalyst is superior to other catalysts under methane-rich conditions (CH_4:O_2 = 11.5:1). This catalyst is quite stable under such high C/O ratios due to the synergistic effect of La and Li oxides. Furthermore, the LiLaNi-Al_2O_3 catalyst keeps stable under the conditions of CH_4:O_2 = 2.2:1 for 300 h at 850 °C. The excellent catalytic activity of this catalyst for the partial oxidation, steam reforming and CO_2 reforming of methane resulted in a high cell performance when a fuel cell with a LiLaNi-Al_2O_3 catalyst layer was operated on either methane-oxygen, methane-H_2O or methane-CO_2 gas mixtures. The LiLaNi-Al_2O_3 catalyst also greatly reduces carbon deposition under pure methane conditions, as compared with the Ni-Al_2O_3 catalyst. The cell with the LiLaNi-Al_2O_3 catalyst layer was stable operated on pure methane at 850 °C for 150 min. The low cost of LiLaNi-Al_2O_3, its excellent catalytic activity and stability and its high coking resistance promise its application for use as the catalyst layer in SOFCs operating on methane.

Acknowledgements

This work was supported by "Outstanding Young Scholar Grant at Jiangsu Province" under contract No. 2008023, program for New Century Excellent Talents in Chinese Ministry of Education (2008), the national basic research program of China under contract No. 2007CB209704, and the National 863 Program under Contract No. 2007AA05Z133.

References

[1] S. McIntosh, R.J. Gorte, Chem. Rev. 104 (2004) 4845–4865.
[2] S. Park, J.M. Vohs, R.J. Gorte, Nature 404 (2000) 265–267.
[3] T. Hibino, A. Hashimoto, T. Inoue, J. Tokuno, S. Yoshida, M. Sano, Science 288 (2000) 2031–2033.
[4] Q.L. Ma, R.R. Peng, Y.J. Lin, J.F. Gao, G.Y. Meng, J. Power Sources 161 (2006) 95–98.
[5] Y.Z. Wu, C. Su, C.M. Zhang, R. Ran, Z.P. Shao, Electrochem. Commun. 11 (2009) 1265–1268.
[6] Y.B. Lin, Z.L. Zhan, J. Liu, S.A. Barnett, Solid State Ionics 176 (2005) 1827–1835.
[7] Y.B. Lin, Z.L. Zhan, S.A. Barnett, J. Power Sources 158 (2006) 1313–1316.
[8] T. Huang, M. Huang, Chem. Eng. J. 138 (2008) 538–547.
[9] T. Huang, M. Huang, Chem. Eng. J. 135 (2008) 216–223.
[10] H.P. He, J.M. Vohs, R.J. Gorte, J. Electrochem. Soc. 150 (2003) A1470–A1475.
[11] C. Lu, W.L. Worrell, J.M. Vohs, R.J. Gorte, J. Electrochem. Soc. 150 (2003) A1357–A1359.
[12] M.D. Gross, J.M. Vohs, R.J. Gorte, J. Electrochem. Soc. 153 (2006) A1386–A1390.
[13] S.W. Tao, J.T.S. Irvine, Nat. Mater. 2 (2002) 320–323.
[14] M. Dokiya, Solid State Ionics 152–153 (2002) 383–392.
[15] J. Meusinger, E. Riensche, U. Stimming, J. Power Sources 71 (1998) 315–320.
[16] W. Sangtongkitcharoen, S. Assabumrungrat, V. Pavarajarn, N. Laosiripojana, P. Praserthdam, J. Power Sources 142 (2005) 75–80.
[17] R. Peters, E. Riensche, P. Cremer, J. Power Sources 86 (2000) 432–441.
[18] T.R. Smith, A. Wood, V.I. Birss, Appl. Catal. A: Gen. 354 (2009) 1–7.
[19] G. Goula, V. Kiousis, L. Nalbandian, I.V. Yentekakis, Solid State Ionics 177 (2006) 2119–2123.
[20] T. Kharlamova, S. Pavlova, V. Sadykov, T. Krieger, G. Alikina, C. Argirusis, Catal. Today 146 (2009) 141–147.
[21] C. Gaudillère, P. Vernoux, C. Mirodatos, G. Caboche, D. Farrusseng, Catal. Today, in press.
[22] N. Nakagawa, H. Sagara, K. Kato, J. Power Sources 92 (2001) 88–94.
[23] Y. Hiei, T. Ishihara, Y. Takita, Solid State Ionics 86–88 (1996) 1267–1272.
[24] M. Pillai, Y.B. Lin, H.Y. Zhu, R.J. Kee, S.A. Barnett, J. Power Sources 195 (2010) 271–279.
[25] D.J. Moon, J.W. Ryu, Catal. Today 87 (2003) 255–264.
[26] Z.L. Zhan, S.A. Barnett, Science 308 (2005) 844–847.
[27] Z.L. Zhan, S.A. Barnett, Solid State Ionics 176 (2005) 871–879.
[28] C.W. Sun, Z. Xie, C.R. Xia, H. Li, L.Q. Chen, Electrochem. Commun. 8 (2006) 833–838.
[29] Z.P. Shao, S.M. Haile, J. Ahn, P.D. Ronney, Z.L. Zhan, S.A. Barnett, Nature 435 (2005) 795–798.
[30] Z.L. Zhan, Y.B. Lin, M. Pillai, I. Kim, S.A. Barnett, J. Power Sources 161 (2006) 460–465.
[31] W. Wang, W. Zhou, R. Ran, R. Cai, Z.P. Shao, Electrochem. Commun. 11 (2009) 194–197.
[32] W. Wang, C. Su, Y.Z. Wu, R. Ran, Z.P. Shao, J. Power Sources 195 (2010) 402–411.
[33] Z.B. Yang, Y.Y. Zhang, W.Z. Ding, Y.W. Zhang, P.J. Shen, Y.D. Zhou, Y. Liu, S.Q. Huang, X.G. Lu, J. Nat. Gas Chem. 18 (2009) 407–414.
[34] S. Natesakhawat, O. Oktar, U.S. Ozkan, J. Mol. Catal. A: Chem. 241 (2005) 133–146.
[35] Z.X. Cheng, Q.L. Wu, J.L. Li, Q.M. Zhu, Catal. Today 30 (1996) 147–155.
[36] M.C. Sánchez-Sánchez, R.M. Navarro, J.L.G. Fierro, Int. J. Hydrogen Energy 32 (2007) 1462–1471.
[37] P. Chen, H.B. Zhang, G.D. Lin, K.R. Tsai, Appl. Catal. A: Gen. 166 (1998) 343–350.
[38] A. Nandini, K.K. Pant, S.C. Dhingra, Appl. Catal. A: Gen. 290 (2005) 166–174.
[39] S.A. Solov'ev, E.V. Gubareni, Y.P. Kurilets, Theor. Exp. Chem. 44 (2008) 268–373.
[40] Q. Miao, G.X. Xiong, S.S. Sheng, W. Cui, L. Xu, X.X. Guo, Appl. Catal. A: Gen. 154 (1997) 17–27.
[41] S.L. Liu, G.X. Xiong, S.S. Sheng, W.S. Yang, Appl. Catal. A: Gen. 198 (2000) 261–266.
[42] S.L. Liu, G.X. Xiong, S.S. Sheng, Q. Miao, W.S. Yang, Stud. Surf. Sci. Catal. 119 (1998) 747–752.
[43] Y.Z. Chen, W. Zhou, Z.P. Shao, N.P. Xu, Catal. Commun. 9 (2008) 1418–1425.
[44] H.X. Gu, R. Ran, W. Zhou, Z.P. Shao, J. Power Sources 172 (2007) 704–712.
[45] R.R. Peng, C.R. Xia, Q.X. Fu, G.Y. Meng, D.K. Peng, Mater. Lett. 56 (2002) 1043–1047.
[46] R.E. Juárez, D.G. Lamas, G.E. Lascalea, N.E. Walsöe de Reca, J. Eur. Ceram. Soc. 20 (2000) 133–138.
[47] A. Tsoga, A. Naoumidis, W. Jungen, D. Stöver, J. Eur. Ceram. Soc. 19 (1999) 907–912.
[48] G.A. El-shobaky, A.M. Ghozza, G.M. Mohamed, Appl. Catal. A: Gen. 241 (2003) 235–245.
[49] X.Y. Chen, Y. Liu, G.X. Niu, Z.X. Yang, M.Y. Bian, A.D. He, Appl. Catal. A: Gen. 205 (2001) 159–172.
[50] J.A.C. Dias, J.M. Assaf, Catal. Today 85 (2003) 59–68.
[51] A.A. Lemonidou, I.A. Vasalos, Appl. Catal. A: Gen. 228 (2002) 227–235.
[52] S. Takenaka, H. Umebayashi, E. Tanabe, H. Matsune, M. Kishida, J. Catal. 245 (2007) 392–400.
[53] S.D. Robertson, B.D. McNicol, H. De Bass, S.C. Kloet, J.W. Jenkins, J. Catal. 37 (1975) 424–431.
[54] J. Requies, M.A. Cabrero, V.L. Barrio, M.B. Güemez, J.F. Cambra, P.L. Arias, F.J. Pérez-Alonso, M. Ojeda, M.A. Peña, J.L.G. Fierro, Appl. Catal. A: Gen. 289 (2005) 214–223.
[55] S.A. Solov'ev, R.N. Zatelepa, E.V. Gubaren, P.E. Strizhak, E.M. Moroz, Activity, Russ. J. Appl. Chem. 80 (2007) 1883–1887.
[56] Z.Y. Hou, O. Yokota, T. Tanaka, T. Yashima, Appl. Catal. A: Gen. 253 (2003) 381–387.
[57] W.G. Schlaffer, C.Z. Morgan, J.N. Wilson, J. Phys. Chem. 61 (1957) 714–722.
[58] M. Pijolat, M. Dauzat, M. Soustelle, Solid State Ionics 50 (1992) 31–39.
[59] S.R. de Miguel, O.A. Scelza, A.A. Castro, Top. Catal. 1 (1994) 87–94.
[60] S.B. Tang, F.L. Qiu, S.J. Lu, Catal. Today 24 (1995) 253–255.
[61] Y. Jiang, A.V. Virkar, J. Electrochem. Soc. 150 (2003) A942–A951.